Optics Communications 459 (2020) 125026

Contents lists available at ScienceDirect

Optics Communications

journal homepage: www.elsevier.com/locate/optcom

Laser generation and amplification of TE and TM modes in a semiconductor optical GaAs waveguide with distributed feedback generated by a space charge wave

Ivan Panyaev, Igor Zolotovskii, Dmitry Sannikov *

Ulyanovsk State University, 432017 Ulyanovsk, Russian Federation

ARTICLE INFO

Keywords:
Semiconductor waveguide
Space charge wave
Laser generation
GaAs

ABSTRACT

We propose a scheme for generating and amplifying coupled optical TE and TM waves in the mid-IR range provided by a grating formed by a space charge wave in a planar waveguide based on GaAs and GaAlAs semiconductors. An undamped harmonic space charge wave with the frequency $\Omega = \omega_m - \omega_n$ (where ω_m and ω_n are the frequencies of the forward and backward optical eigenwaves) can be formed in a longitudinal constant electric field in the predomain mode. The coupling coefficients for the optical TE and TM modes of the perturbed n-GaAs waveguide have been obtained. For pairs of the TE and TM modes of the same indices ($m = n$), the reflectance and transmittance dependences on the carrier concentration and pump level have been found. Generation of the forward and backward waves at a wavelength of 10.6 μm is shown for TE_0 and TM_2 modes at the gain factor of $\gamma \approx 152$ cm^{-1} and 155 cm^{-1}, respectively. The obtained results can be used to create semiconductor two-frequency coherently synchronized oscillators based on space charge wave–optical mode interaction.

1. Introduction

The term "space charge wave" (SCW) originates from the microwave technology to denote a wave-like propagation of perturbations of the space charge density and velocity in an electron beam [1–3]. In semiconductor physics, SCW is associated with spatio-temporal charge density perturbations arising in semiconductors with the negative differential mobility in strong electric fields [4–6]. When SCW propagates in a semiconductor crystal, deviation of the concentration of free charge carriers n_1 from the equilibrium concentration n_0 occurs. This leads to a periodic change in the dielectric constant with a modulation depth sufficient for an effective interaction between SCW and optical modes. As a result of inter-valley electron transfer, the differential conductivity of the sample becomes negative, thereby enabling generation and amplification of eigenspace charge waves [7]. The generated SCWs could propagate at the velocity close to that of the carrier drift (of the order of 10^7 cm/s).

The effect of SCW amplification in semiconductor films is employed, in particular, in traveling-wave amplifiers [8–10]. In Ref. [11], SCWs have been proposed to control the electromagnetic waves in semiconductor films. The theory of SCWs and effective method of their excitation based on illumination of the crystal by a traveling interference pattern are considered in [12–14]. SCW could be used to create photorefractive gratings in electro-optical crystals [15], realize the superheterodyne amplification of THz electromagnetic waves [16,17] and parametric interaction [18,19] in thin-film n-GaAs structures. Note that the frequency range of the amplified SCW in GaAs films is $f \leq 50$ GHz. In order to expand this frequency range up to $f \leq 500$ GHz, the n-GaN and n-InN thin film based waveguides have been proposed [20]. However, the III-nitrides suffer from the higher critical fields ($E_c \approx 100$ kV/cm against the 3 kV/cm in n-GaAs). In a series of works [21–25], the dispersion properties of SCW propagating in a semiconductor waveguide have been analyzed. Also, an effective collinear interaction of optical waveguide modes with SCWs traveling and amplifying in amplitude has been explored under various boundary conditions.

In contrast to papers [21,23,25], where SCW amplifying in amplitude is studied, this paper considers SCW traveling along a n-GaAs waveguide without amplification and absorption. Besides, we investigate the amplification and generation regimes of the TE and TM optical waves with an external optical pumping. SCW forms a periodic grating in the semiconductor films providing interaction between the forward and backward waves at ω_m and ω_n. The phase mismatching providing generation of the forward and backward waves without end reflectors has been analyzed.

2. Statement of the problem

The waveguide structure consists of the substrate (1), semiconductor n-GaAs film (2) of the thickness t_{WG} and coating layer 3. In the

* Correspondence to: Ulyanovsk State University, 432017, 42 L.Tolstoy str., Ulyanovsk, Russian Federation.
E-mail address: sannikov-dg@yandex.ru (D. Sannikov).

https://doi.org/10.1016/j.optcom.2019.125026
Received 10 August 2019; Received in revised form 22 November 2019; Accepted 25 November 2019
Available online 28 November 2019

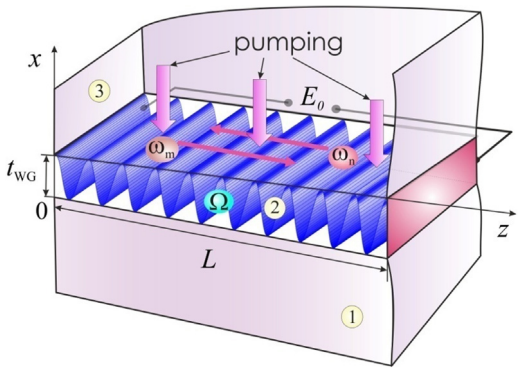

Fig. 1. 3D geometry of the structure. Interaction of the forward and backward optical waves and SCW at the frequencies ω_m, ω_n and Ω, respectively.

absence of perturbations, the dielectric constants of layers are ε_1, ε_2 and ε_3, respectively. The x-axis is perpendicular to the media interface. A constant electric field E_0 applied to the structure along the z-axis creates a perturbation of the dielectric constant $\Delta\varepsilon(z)$. The electrodes are spaced by the distance L (the length of the mode interaction region) and can be made of a transparent material, e.g., InGaBiAs:Si [26,27] (see Fig. 1).

To obtain the SCW generation regime in a semiconductor layer, the Krömer condition [28] has to be satisfied. For GaAs it has the form $10^{10} \le n_0 L \le 10^{12}$ cm^{-2}, where n_0 is the equilibrium concentration of charge carriers [29,30]. By choosing the doping concentration of the waveguide layer and its length, the value of the applied field E_0, which in n-GaAs should exceed a threshold value of $E_t \approx 3$ kV/cm, an electron grating induced by SCW (without switching to the Gunn domain mode) could be created [10,29,31].

3. Space charge waves in n-GaAs film

In order to describe the wave perturbations of the electron flow in a semiconductor film, the Poisson equation and the equation for the total current are required. Using the quasistatic approximation ($\mathrm{rot}\mathbf{E}_1 = 0$) as well as the electrodynamic boundary conditions, we can obtain the dispersion equation relating the SCW wave number Q and the frequency Ω [10]:

$$DQ^2 + i\,(\Omega - Qv_0) + \mu_d\omega_M = 0, \tag{1}$$

where $\mu_d = \mu_0^{-1}(dv/dE)$ is the negative differential mobility, μ_0 is the mobility of "unheated" electrons, $\omega_M = 4\pi e n_0\mu_0/\varepsilon_2$ is the Maxwell relaxation frequency corresponding to the electroneutrality loss time of the semiconductor, e is the electron charge, v_0 is the speed of "hot" carriers. Two solutions of Eq. (1) correspond to the direct (drift) and reverse (diffusion) SCW. Further, the direct SCW is considered only since the reverse wave decays rapidly [5].

Eq. (1) shows that SCW propagates without absorption (or amplification) at the frequency

$$\Omega = v_0 Q = v_0\sqrt{-\mu_d\omega_M/D}, \tag{2}$$

where D is the diffusion coefficient. In this case, the coordinate dependence of the SCW perturbation of the dielectric constant in a semiconductor layer can be represented by the function:

$$\Delta\varepsilon(z) = \frac{1}{2}\Delta\varepsilon\{\exp[i(\Omega t - Qz)] + c.c.\}, \tag{3}$$

where $Q = 2\pi/\Lambda$ and Λ is the period of the grating induced by SCW. As shown in [22,31], the modulation depth of the dielectric permittivity in a waveguide film is

$$\Delta\varepsilon \approx \left|e\varepsilon_2 E_1 Q/m^*\omega^2\right| \tag{4}$$

where E_1 is the amplitude of the perturbing electric field in a semiconductor in the predomain mode, m^* is the electron effective mass, ω is the light frequency. The permittivity modulation depth value of $\Delta\varepsilon \approx 10^{-5}$ has been reported (see [31]) for a crystal (n-GaAs) at the optical wavelength of $\lambda = 10.6$ μm with $m^* \approx 0.063m_0$ ($T = 300$ K), where m_0 is the mass of free electrons, $\varepsilon_2 \approx 12$, $E_1 \approx 300$ V/cm ($E_1 \ll E_0$).

4. Optical waveguide modes

In the amplification scheme, the forward optical wave can be introduced into the waveguide (from the outside of the interaction region L) through the prism or grating coupling element providing selective excitation of the mth waveguide mode. The mode order is selected by changing the incident angle of the laser beam. Similarly, the backward optical wave could be extracted from the structure [32,33]. The frequencies of the forward, backward optical waves, and SCW, all moving along the z-axis, are related as $\omega_m = \omega_n + \Omega$.

TE modes with the wave field components (H_x, E_y, H_z) and TM modes with the components (E_x, H_y, E_z) are the eigenwaves of the unperturbed structure. Profile functions for waveguide modes, i.e. distributions of the y-component over the x-coordinate have the form

$$F_{ym}(x) = \begin{pmatrix} E_{ym}(x) \\ H_{ym}(x) \end{pmatrix} = C_m \cdot \begin{cases} \exp(-qx), & x \ge 0, \\ [\cos hx - \dfrac{\zeta q}{h}\sin hx], & -t_{WG} \le x \le 0, \\ [\cos ht_{WG} + \dfrac{\zeta q}{h}\sin ht_{WG}]\exp[p(x + t_{WG})], & x \le -t_{WG}, \end{cases} \tag{5}$$

where $\zeta = 1$ and $\zeta = \varepsilon_2/\varepsilon_3$ are for the TE and TM modes, respectively. The transverse components of the wave vector in each layer are $p^2 = \beta_m^2 - k_0^2\varepsilon_1$, $h^2 = k_0^2\varepsilon_2 - \beta_m^2$, $q^2 = \beta_m^2 - k_0^2\varepsilon_3$, β_m is the propagation constant of the mth mode and $k_0 = \omega/c$ is the wave number of the electromagnetic wave. The constant C_m has units of (erg/cm^3)$^{1/2}$ and is determined from the power normalization condition for the mth mode in the structure:

$$P_0 = \frac{\beta c a_y}{8\pi k_0 \Gamma}\int_{-\infty}^{\infty}\left[F_{ym}(x)\right]^2 dx = 1\,[\mathrm{erg/s}], \tag{6}$$

where $a_y = 1$ cm is the normalization length along the y-axis, $\Gamma = 1$ for TE modes and $\Gamma = \varepsilon_2$ for TM modes. Integrating Eq. (6), we obtain

$$C_m = 4h\left\{\frac{\pi k_0\Gamma P_0}{\beta_m c\, a_y [h^2 + (\zeta q)^2]\, t_{eff}}\right\}^{1/2}. \tag{7}$$

Here, the effective waveguide thickness is introduced for the mth mode

$$t_{eff} = t_{WG} + \frac{\zeta}{q}\frac{(q^2 + h^2)}{(\zeta q)^2 + h^2} + \frac{\eta}{p}\frac{(p^2 + h^2)}{(\eta p)^2 + h^2}, \tag{8}$$

where $\eta = 1$ and $\eta = \varepsilon_2/\varepsilon_1$ are for TE and TM modes, respectively.

The dispersion equation for a 3-layer unperturbed waveguide has the form (see [33,34])

$$h\,t_{WG} - \pi m - \arctan\left(\frac{\zeta q}{h}\right) + \arctan\left(\frac{\eta p}{h}\right) = 0. \tag{9}$$

When a longitudinal electric field E_0 is switched on, a periodically modulated inhomogeneity arises in the form of an SCW grating leading to mode coupling. The total wave field for the TE and TM modes in such a perturbed waveguide can be written as

$$F_y(x, z) = \sum_{m=1}^{M}\left(A_m(z)\exp[-i\,\beta_0 z] + B_m(z)\exp[i\,\beta_0 z]\right)F_{ym}(x), \tag{10}$$

where $A_m(z)$ and $B_m(z)$ are the dimensionless amplitudes of the forward and backward traveling waves, M is the total number of guided

modes in the structure. In relation (10), the radiation modes forming a continuum are neglected [35,36]. "Resonant" propagation constant

$$\beta_m = \beta_0 = \frac{\pi l}{\Lambda} \tag{11}$$

provides a coupling between modes with close frequencies and phase-matching, where l is the Bragg diffraction order.

In terms of the coupled mode theory [35,37], the coupling coefficients can be obtained for TE and TM waveguide modes with the same indices ($m = n$):

$$\kappa_{mm}^{TE} = \frac{\Delta\varepsilon\,\omega\,a_y}{32\pi\,P_0}\frac{C_m^2}{2\varepsilon_2\,h^2}\left[t_{WG}[h^2+(\zeta q)^2]+\frac{(\eta p+\zeta q)\,(h^2+\zeta\eta pq)}{h^2+(\eta p)^2}\right], \tag{12a}$$

$$\kappa_{mm}^{TM} = \frac{a_1}{4\beta_0}\frac{\beta_0^2\int_{-t_{WG}}^{0}[H_{ym}(x)]^2dx-\int_{-t_{WG}}^{0}[\partial_x H_{ym}(x)]^2dx}{\int_{-\infty}^{\infty}\varepsilon_2^{-1}\,[H_{ym}(x)]^2dx}, \tag{12b}$$

where $\partial_x \equiv \partial/\partial x$ and the expansion coefficient ($l = 1$) in the Fourier series for a harmonic disturbance Eq. (3) is determined by the expression

$$a_1 = \frac{4}{\Lambda}\int_0^{\Lambda/2}\frac{1}{\varepsilon_2+\Delta\varepsilon\cos(Qz)}\cos(Qz)\,dz = \frac{2}{\pi}\int_0^{\pi}\frac{\cos u}{\varepsilon_2+\Delta\varepsilon\cos u}du. \tag{13}$$

5. Mode coupling equations and their solution

Following [35], the coupling equations for guided counterpropagating eigenwaves of the perturbed waveguide in the presence of amplification γ [cm^{-1}] can be written as:

$$\begin{aligned} dA/dz &= -i\,\kappa_{mn}B\exp[2i\Delta\beta z]+\gamma A,\\ dB/dz &= i\,\kappa_{mn}^{*}A\exp[-2i\Delta\beta z]+\gamma B. \end{aligned} \tag{14}$$

Here, the detuning of the propagation constants from the resonance value $2\Delta\beta = \beta_m + \beta_n - Q$ is introduced. For simplicity, the amplitudes are expressed as $A(z) = A'(z)\exp(\gamma z)$ and $B(z) = B'(z)\exp(-\gamma z)$. Hence, Eq. (14) have the following solutions

$$\begin{aligned} &A'(z)\exp[-i(\beta_m - Q + i\gamma)z]\\ &\quad = A(0)\frac{(\gamma - i\Delta\beta)\sinh[S\,(L-z)] - S\cosh[(S(L-z))]}{(\gamma - i\Delta\beta)\sinh(SL) - S\cosh(SL)},\\ &B'(z)\exp[i(\beta_m - Q + i\gamma)z] = A(0)f\frac{-i\kappa_{mm}\sinh[(S(L-z))]}{(\gamma - i\Delta\beta)\sinh(SL) - S\cosh(SL)}. \end{aligned} \tag{15}$$

Here, an additional parameter $S = \sqrt{|\kappa_{nm}|^2 + (\gamma - i\Delta\beta)^2}$ has been introduced. The solutions of Eq. (7) gives the energy reflection and transmission coefficients of the modes in a waveguide with an interaction region of the length L:

$$\begin{aligned} R &= \left|\frac{F_r(0)}{F_i(0)}\right|^2 = \left|\frac{B'(0)}{A(0)}\right|^2 = \left|\frac{\kappa_{mn}\sinh SL}{(\gamma - i\Delta\beta)\sinh(SL) - S\cosh(SL)}\right|^2,\\ T &= \left|\frac{F_i(L)}{F_i(0)}\right|^2 = \left|\frac{A'(L)}{A(0)}\right|^2 = \left|\frac{S}{(\gamma - i\Delta\beta)\sinh(SL) - S\cosh(SL)}\right|^2. \end{aligned} \tag{16}$$

The amplitudes of electric (for TE polarization) and magnetic (for TM polarization) fields $F_r(0)$, $F_i(0)$ and $F_i(L)$ correspond to the backward wave at the beginning of a perturbed region, the forward wave at the beginning and at the end of an interaction region, respectively. When the waveguide film is pumped, the waveguide segment L works as an amplifier for the reflected and transmitted waves. Importantly, relations (16) describe the reflection and transmission coefficients of waves in the corrugated-waveguide laser [35] and fundamentally are different from the case of parametric amplification [38–40]. Also, Eq. (16) can be employed to study the conditions for generation of the optical waves through SCW–optical interaction.

Table 1
Sellmeier coefficients for the guiding layer material.

f_j, units	$f_1^{(1)} = 5.372514$	$f_2^{(1)} = 0.0242996$	$f_3^{(1)} = 1.957522$
λ_j, μm	$\lambda_1^{(1)} = 0.1567$	$\lambda_2^{(1)} = 0.01375$	$\lambda_3^{(1)} = 0.22715$

6. Numerical analysis and discussion

Let us numerically analyze the SCW–optical interaction for a n-GaAs guiding film with the refractive index dispersion [41]

$$\varepsilon_2(\lambda) = 5.372514 + \sum_{j=1}^{3}\frac{f_j\,\lambda^2}{\lambda^2 - \lambda_j^2}. \tag{17}$$

The empirical coefficients in Eq. (17) are listed in Table 1.

For the substrate and coating, $Al_xGa_{1-x}As$ with the refractive index of $n_1 \approx$ 3demonstrating relatively low losses within the operating wavelength range of 1–11 μm has been taken [42]. In fact, the carrier drift velocity depends on the external field E_0. Therefore, to simulate the experimental dependence $v_0(E_0)$, the function and fitting parameters for GaAs have been borrowed from [10]. Let us estimate the SCW frequency for typical values of the parameters: mobility of "unheated" electrons $\mu_0 = 8500$ cm^2/(V s), static electric field strength $E_0 = 4.9$ kV/cm, diffusion coefficient $D = 207$ cm^2/s [6], and equilibrium concentration $n_0 = 10^{13}$ cm^{-3}. For these parameters, the electron drift velocity is $v_0 \approx 1.88\cdot 10^7$ cm/s, differential mobility is $\mu_d = -0.254$, the SCW wave number at a wavelength of $\lambda = 10.6$ μm is $Q \approx 4200$ μm^{-1}, and according to relation (2) the frequency is $\Omega \approx 3.6\cdot 10^{11}$ s^{-1}. Noteworthy, in a real experiment, in order to avoid the domain-type instabilities in a sample the additional measures, like the load resistance matching, may be needed [10,30].

Fig. 2(a) shows the wavelength dependences of the effective refractive indices $n_m^* = \beta_m/k_0$ of TE and TM modes. The region of existence of the effective mode refractive indices is quite wide and is limited by the difference in the values of asymptotes n1 = 3 and $n_2(\lambda)$. Due to the waveguide structure symmetry, the values n_m^* for TE and TM modes of the same order are slightly different, while the zero-order modes, in accordance with Eq. (9), do not have a cutoff. The first three modes with indices $m = 0, 1, 2$ exist in the whole considered wavelength region. With the wavelength increase, the eigenwaves experience a cutoff (violation of total internal reflection). At shorter wavelengths, the number of propagating modes increases and the total number of modes is defined as

$$m_{\max} = \left\{\left(t_{WG}k_0\sqrt{n_2^2-n_1^2} - \arctan\sqrt{(n_1^2-n_3^2)/(n_2^2-n_1^2)}\right)/\pi\right\}_{int} + 1, \tag{18}$$

where "int" is an integer part of the expression. At the selected parameters at the minimum wavelength of 1 μm, the maximum number of TE and TM modes reaches 37.

Fig. 2(b) shows the wavelength dependences of the coupling coefficients (overlap integrals) for TE and TM modes of the same order ($m = n$). For both TE and TM polarizations, the coupling coefficients grow with increasing wavelength and, reaching a maximum value, tend to zero when approaching the cutoff. In the case of TM polarization, however, for $m = n = 0$ the coupling coefficient crosses zero at $\lambda \approx$ 10.6 μm and becomes negative with the increasing wavelength.

Unlike TE polarization, for which the maximum value of the overlap integral decreases with increasing mode index, the opposite relationship is observed for TM-polarized modes: the maximum value of the coupling coefficient increases with an increasing mode index.

The coupling coefficient dependences on the waveguide layer thickness t_{WG} are shown for the TE and TM pairs of modes with the same order ($m = n$) in Fig. 3(a) and Fig. 3(b), respectively. The modes of different orders demonstrating lower coupling effectiveness than those of the same order are neglected [24]. In general, the coupling

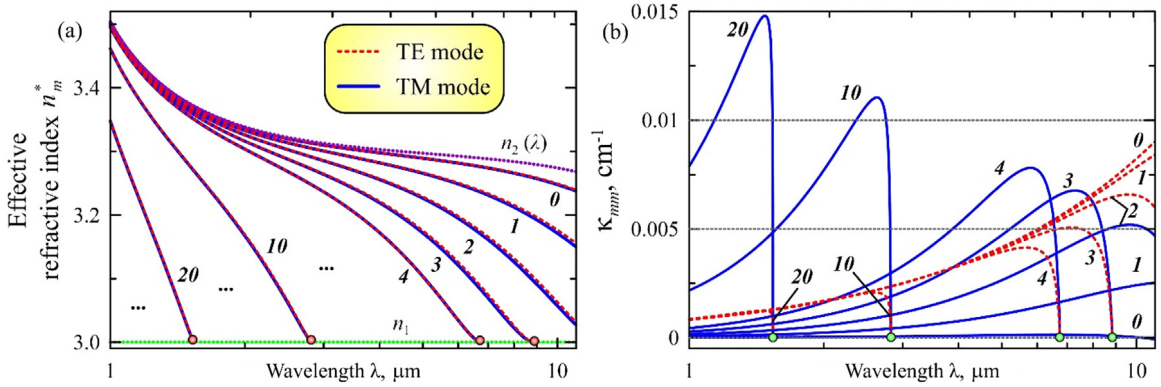

Fig. 2. Dispersion of effective refractive indices (a) and coupling coefficients (b) for TE and TM modes in an unperturbed n-GaAs waveguide with a film thickness of t_{WG} = 10 μm. The numbers correspond to the mode orders $m = n$ = 0, 1, 2, 3, 4, 10 and 20.

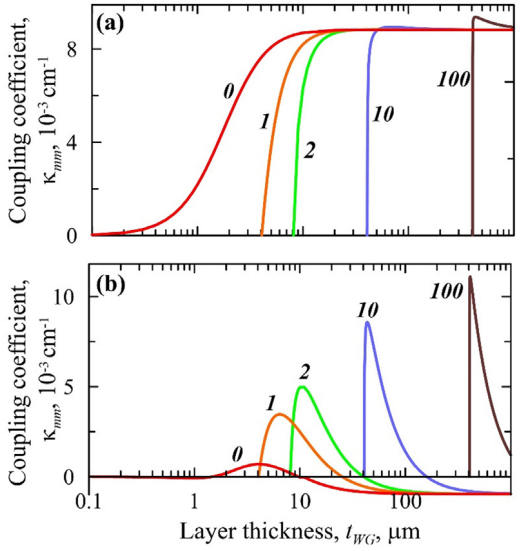

Fig. 3. The coupling coefficients of pairs of TE and TM modes of the same order in an n-GaAs waveguide with $n_0 = 10^{13}$ cm^{-3}. Fig. (a) and (b) – TE and TM modes at λ = 10.6 μm, external field E_0 = 4.9 kV/cm. The numbers correspond to the mode orders $m = n$ = 0, 1, 2, 10 and 100 (curves *1*, *2*, *3*, *10* and *100*).

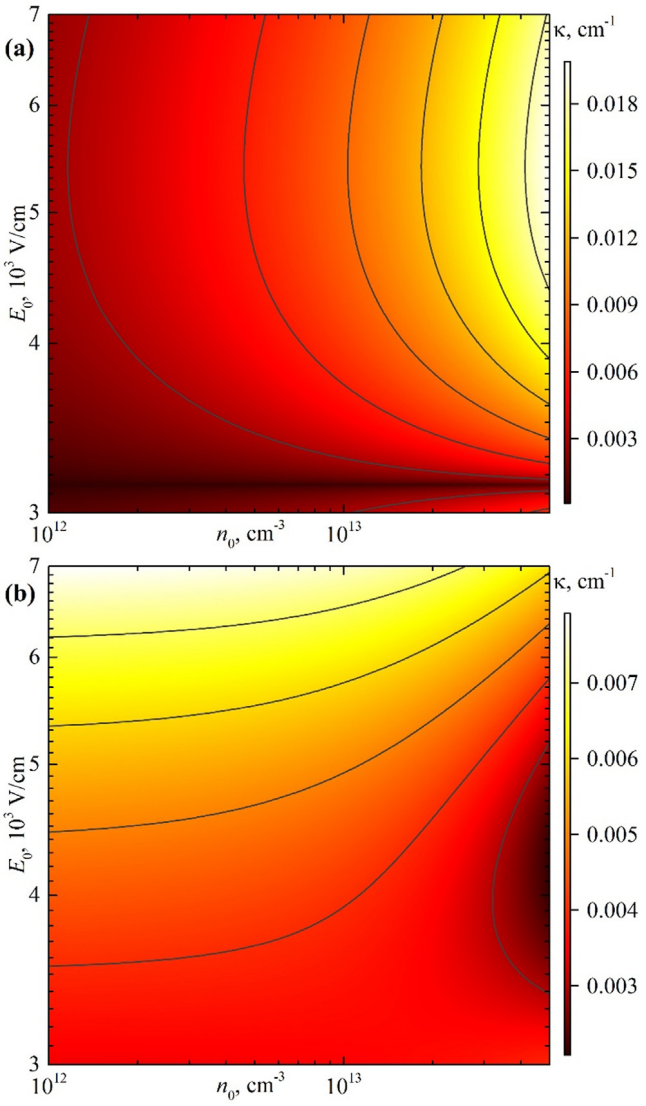

Fig. 4. Dependences of the coupling coefficients on the electron concentration in the n-GaAs film and on the external field for TE [$m = n$ = 0, (a)] and TM [$m = n$ = 2, (b)] modes; λ = 10.6 μm, film thickness t_{WG} = 10 μm.

coefficients of both TE and TM modes change rapidly near the cutoff (at small thicknesses) and have maxima that are higher for higher order modes. Far from the cutoff, the coupling coefficients for TE modes grow and tend to a constant value. As Fig. 2(b) shows, the coupling coefficients κ_{mm}^{TM} for TM modes cross zero and asymptotically tend to a small negative value of the order of 10^{-3} cm^{-1}. This value corresponds to the coupling coefficient of TM modes in the approximation of a waveguide with infinite thickness $(t_{WG}\to\infty)$. Importantly, the coupling coefficient for the zeroth TM mode crosses zero twice (near t_{WG} = 1.5 and 10 μm). Mathematically, this is due to the annihilation of terms with different signs in relation (12b), and physically this means that due to the resonance condition a situation of "uncoupling" is possible when co- and counter propagating TM modes of the zero order are not coupled anymore.

Fig. 4 demonstrates the dependence of the coupling coefficients on the equilibrium concentration n_0 and external field E_0 in the structure with a fixed thickness of the guiding film for TE_0 and TM_2-modes at λ = 10.6 μm. In this case, the coupling coefficients reach the higher values in comparison with modes of other orders.

The coupling coefficients for the TE_0 mode grow with increasing carrier concentration and reach the maximum value at $E_0 \approx 5.5$ kV/cm in the considered range of parameters [Fig. 4(a)]. One can see the κ_{00}^{TE} domain where the coupling coefficient is small and almost independent of the electron concentration (a dark horizontal band in vicinity of $E_0 \approx 3.1$ kV/cm). For TM_2 modes [Fig. 4(b)], the coupling coefficient

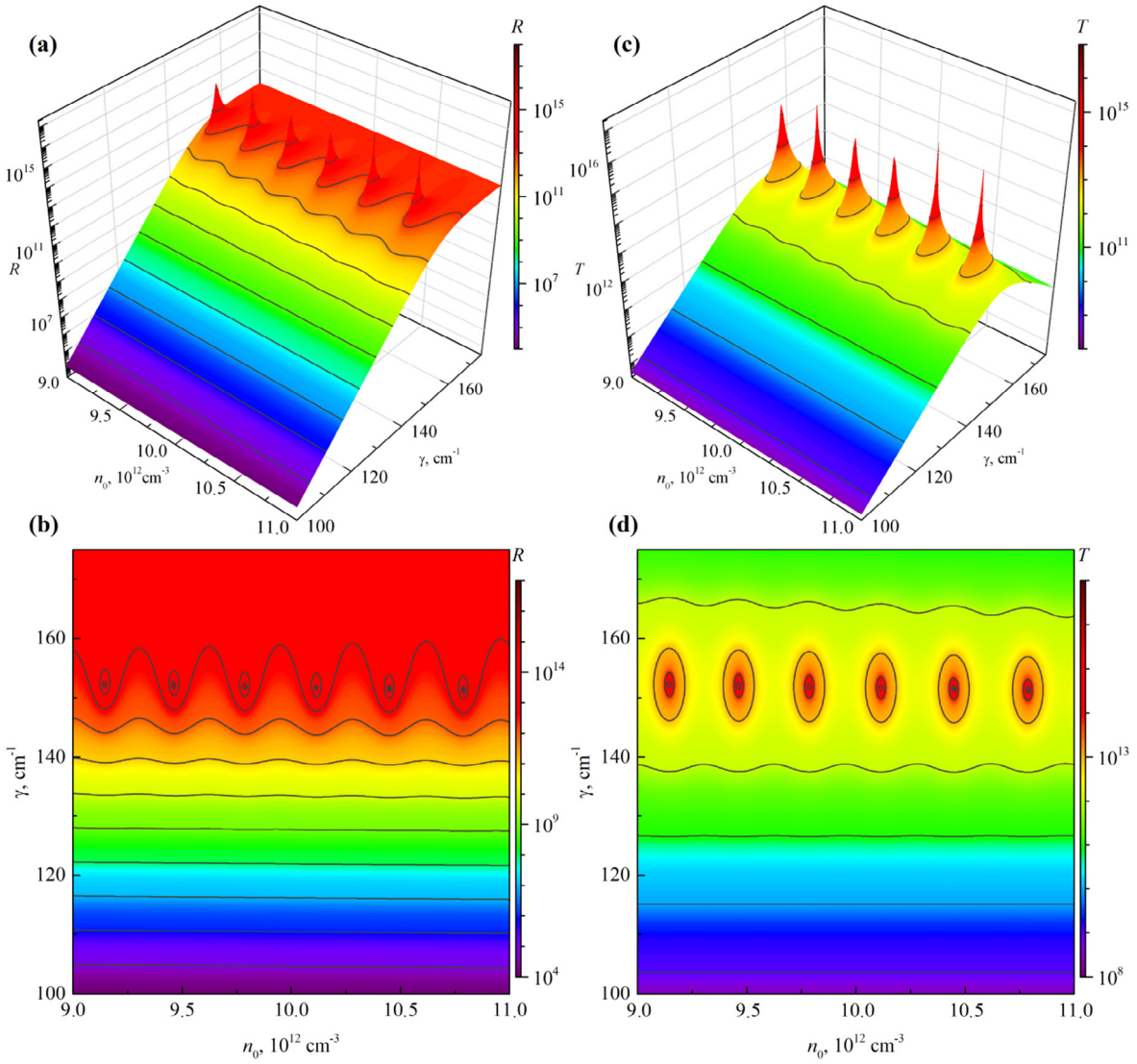

Fig. 5. Reflection gain $R(0)$ in the $n_0 - \gamma$ plane for the inverse [(a), (b)] and transmission gain $T(L)$ for the direct [(c), (d)] TE_0 mode at a wavelength $\lambda = 10.6$ μm. (b, d) are the top view; film thickness $t_{WG} = 10$ μm, $L = 0.1$ cm.

is in strong dependence on the external field but slightly depends on the concentration. With the concentration increase, higher values of the external field are required to maintain a constant value of the coupling coefficient.

In this case, the condition of the SCW existence is determined by the length of the interaction region. For example, for the interaction length $L = 0.1$ cm the concentration of free carriers n_0 in the film below 10^{13} allows us to satisfy the limiting Krömer condition $n_0 L = 10^{12}$ cm^{-2} and avoid establishment of the domain regime. Noteworthy, a multi-domain mode could be used to increase the modulation depth of the dielectric constant, though it is beyond the scope of this paper. In this case, the main difficulty is to find the appropriate boundary conditions and stabilization of the Gunn oscillations shape [6].

Figs. 2–4 show that due to the low depth of dielectric permittivity modulation ($\Delta\varepsilon \approx 10^{-5}$), the coupling coefficients of the TE and TM modes of the same order do not exceed $\sim 10^{-2}$ cm^{-1} that is 3 orders of magnitude lower than those in the corrugated waveguide structures (e.g., [37,43]). Below, we will show that the generation can be obtained even at such low values of the overlap integrals.

To analyze the amplification and generation modes, isolines (i.e. contours of equal reflection and transmission gain) are constructed using Eq. (16) for the backward and forward TE_0 and TM_2 modes (coupled via the first diffraction order with the counter propagating modes of the same index) as functions of the free carrier concentration and gain factor in the proximity of the region the Krömer criterion is fulfilled for the given parameters (Figs. 5 and 6).

Fig. 5 demonstrates that the singularity points, where the coefficients R and T values are above 10^{14}, correspond to a series of generated modes. Each subsequent laser mode arises with an increase in the carrier concentration n_0 by approximately $6 \cdot 10^{11}$ cm^{-3}. In this case, the required gain factor is about 152 cm^{-1}. With a further increase in the optical pumping level, the backward wave maintains a high reflection gain of about $\sim 10^{13}$, whereas for the forward wave, a decrease of the transmission gain down to $\sim 10^{11}$ is observed. Thus, in the considered structure, the laser modes can be generated by SCW–optical mode interaction without the use of end reflectors.

Periodicity of the generation peaks governs the waveguide structure. Therefore, it can be tuned by changing the external parameters, such as external field, temperature, etc. The characteristics of the waveguide resonator providing an effective generation at 10.6 μm are listed in Table 2.

When the tunable CO_2 laser is used for pumping, [44–46], the Raman shift is about several THz [47]. Following [48,49], we can assign the 3rd order nonlinearity coefficient $\mathrm{Re}[\chi^{(3)}] \approx 10\text{^}(-5)$ esu for GaAs that gives [50] the value of nonlinear refractive index $\tilde{n}_2 \approx 10^{-8}$ cm^2/W for $\lambda \approx 10.6$ μm. Therefore, to obtain the gain $\gamma \approx 150$ cm^{-1},

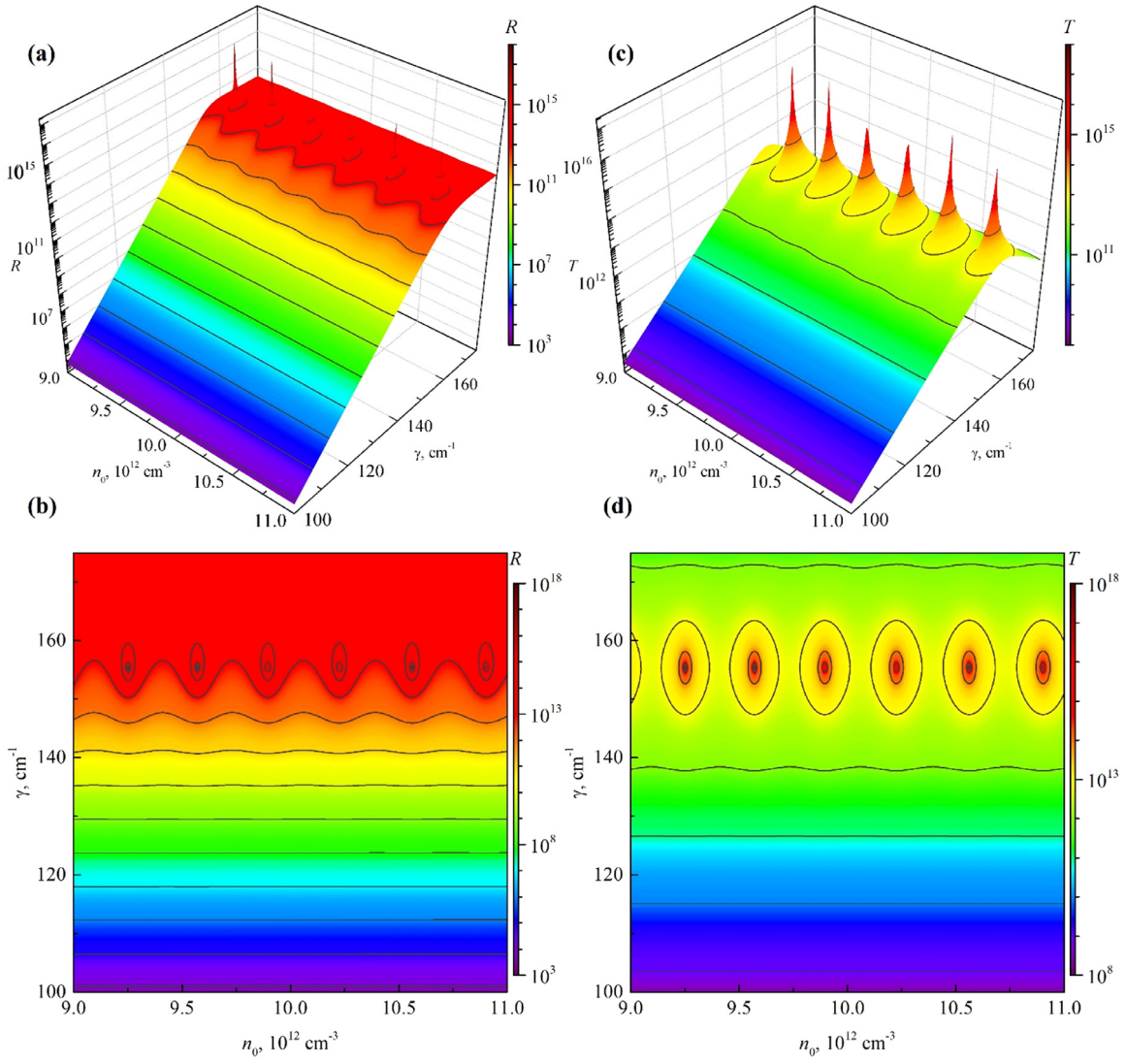

Fig. 6. Reflection gain $R(0)$ in the $n_0 - \gamma$ plane for the inverse [(a), (b)] and transmission gain $T(L)$ for the direct [(c), (d)] TM_2 mode at a wavelength $\lambda = 10.6$ μm. (b, d) are the top view; film thickness $t_{WG} = 10$ μm, $L = 0.1$ cm.

Table 2
The optimal parameters of the waveguide and radiation for the SCW–optical coupling and laser generation of the forward and backward waves.

Wavelength λ, μm	Mode	Doping concentration of the n-GaAs film n_0, cm^{-3}	Film thickness t_{WG}, μm	Interaction length L, μm	Gain factor γ cm^{-1}	Propagation constant detuning $\Delta\beta$, μm^{-1}	Intermode coupling coefficient κ_{mm}, cm^{-1}
10.6	TE_0 TM_2	10^{13}	10	1000	152 155	1.73 1.61	0.0087 0.0057

the pumping intensity $I \approx 10^6$ W/cm^2 is required that is below the intensities applied in [51] for supercontinuum generation in the mid-IR.

Stability of laser feedback can be ensured by controlling the electric field E_0, which, in turn, affects the period of the dynamic SCW grating. Importantly, in our case of the continuous-wave generation in a planar waveguide, the wave diffraction is compensated (at least partially) by reflections from the waveguide walls [52].

It is important to note that with a wavelength decrease the permittivity ε_2 increases leading to an increase in detuning value $\Delta\beta$. Hence, Figs. 5 and 6 show that lasing peaks for the TM_2 mode arise at higher gain levels than for the TE_0 mode.

Besides, the small modulation depth of the permittivity (in this case, $\Delta\varepsilon \approx 10^{-5}$) and significant mismatch of the propagation constants $2\Delta\beta = 2\beta_m - Q$ also require sufficiently high level of pumping. Although the required value of γ is comparable with the threshold gain factor ($\gamma \approx 100$ cm^{-1}) in corrugated waveguide lasers [35,43], the advantage of the proposed waveguide generation scheme is the ability to control the parameters of the SCW grating.

Fig. 7 shows the dependences of the amplitude moduli of the forward and backward waves on the z-coordinate [Eq. (15)] inside the structure with the parameters enabling generation of the TE_0-TE_0 and TM_2-TM_2 pairs of modes at $\lambda = 10.6$ μm. Wave directions are indicated by filled arrows. In general, at $A(0) = 0$, Eq. (15) gives zero values for the amplitudes of the forward and backward waves. However, generation can occur without an input signal from the noise. In this case, we have to assign $A(0) = 1$.

As can be seen from insets on Fig. 7, the amplitudes of the forward and backward waves of both polarizations oscillate near the initial boundaries ($|A(0)|$ and $|B(L)|$). Mathematically, these oscillations arise due to the appearance of periodic functions (sines and cosines) in

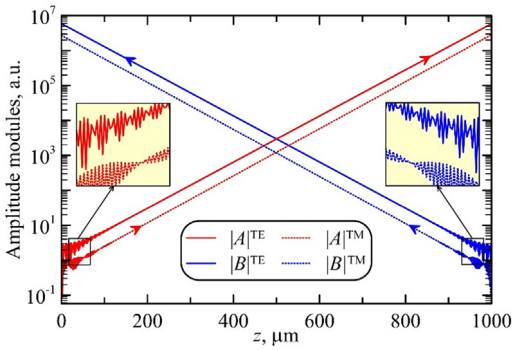

Fig. 7. Distributions of amplitude moduli along the waveguide length for the forward and backward waves ($|A(z)|$ and $|B(z)|$, respectively) of different polarizations at $\lambda = 10.6$ μm, $t_{WG} = 10$ μm, $E_0 = 5.5$ kV/cm^2, $L = 0.1$ cm. TE-polarization (solid lines): mode numbers $m = n = 0$, $\gamma = 152$ cm^{-1}; TM-polarization (dotted lines): $m = n = 2$, $\gamma = 155$ cm^{-1}.

the real and imaginary parts of complex amplitudes. Physically, these oscillations reflect both the amplification process as a result of the interaction between the forward and backward waves and the process of generation from noise. The amplitude and frequency of the oscillations depends on the polarization and proximity to the generation peak.

In the proposed scheme, the dominant noise in the laser amplifier is the beat noise between the components of spontaneous emission and the beat noise between the signal and spontaneous emission at the level below −40 dBm and above −40 dBm from the input signal, respectively (commonly, the beat noise is dominating over the shot noise [53]). In addition, shot noise can appear at the contacts of the electrodes when generating an SCW. In our case, at the proper pump level (and corresponding gain factor), the generation arises from noise (see Figs. 5, 6, 7), so there is no need to introduce a weak signal beam from an external source. It is worth noting that the pulsed pumping can be used for the considered waveguide structure. However, it is beyond the scope of this paper.

7. Conclusions

The conditions for amplification and two-frequency generation of difference-frequency synchronized optical radiation in a semiconductor waveguide based on n-GaAs are found. We have determined the solid-state parameters satisfying the Krömer criterion $n_0 L = 10^{12}$ cm^{-2}, thus avoiding the domain regime in the n-GaAs film. The reflection and transmission gain have been studied for pairs of counterpropagating TE and TM modes of the same order with the highest coupling coefficients in the middle infrared region (for TE_0- and TM_2-modes at a wavelength of 10.6 μm). The conditions for lasing at the gain factor of $\gamma \approx 152$ cm^{-1} for TE modes and $\gamma \approx 155$ cm^{-1} for TM modes and corresponding detuning from phase synchronism are found. The presence of a controlled SCW grating in the proposed scheme makes it advantageous over a corrugated waveguide laser or orientation-patterned-GaAs elements [54–56]. One should note that the SCW difference-frequency tuning can be achieved by an optimal balancing between the doping concentration in semiconductor, amplitude and polarity of the external electric field E_0, and temperature. In order to ensure a stability of the SCW in the experiment, additional measures could be required, such as matching of load resistance and maintaining the temperature regime. The results can be used to create two-frequency semiconductor laser emitters in the middle infrared region based on space charge wave–optical mode interaction.

CRediT authorship contribution statement

Ivan Panyaev: Software, Visualization, Writing - original draft, Writing - review & editing, Investigation. **Igor Zolotovskii:** Conceptualization, Writing - original draft, Writing - review & editing, Project administration. **Dmitry Sannikov:** Software, Visualization, Investigation, Writing - original draft, Writing - review & editing, Supervision.

Acknowledgments

The authors would like to thank Dr. K.V. Borisova for help in translating the text into English. This work was supported by the Ministry of Education and Science of the Russian Federation [Grants No. 3.8154.2017/BP (I.P., D.S),] and Russian Fund of Fundamental Research No. 18-29-19101 (I.P., I.Z).

References

[1] S. Ramo, Space charge and field waves in an electron beam, Phys. Rev. 56 (1939) 276–283, http://dx.doi.org/10.1103/PhysRev.56.276.
[2] J.E. Rowe, Nonlinear Electron-Wave Interaction Phenomena, Academic Press, 1965.
[3] S. Ramo, J.R. Whinnery, T. Van Duzer, Fields and Waves in Communication Electronics, third ed., John Wiley & Sons, 1994.
[4] H. Kroemer, Nonlinear space-charge domain dynamics in a semiconductor with negative differential mobility, IEEE Trans. Electron Devices ED-13 (1966) 27–40, http://dx.doi.org/10.1109/T-ED.1966.15631.
[5] A.A. Barybin, Waves in Thin-Film Semiconductor Structures with Hot Electrons, Nauka, Moscow, 1986 (in Russian).
[6] M. Shur, GaAs Devices and Circuits, Plenum Press, New York, 1987.
[7] B.K. Ridley, T.B. Watkins, The possibility of negative resistance effects in semiconductors, Proc. Phys. Soc. 78 (1961) 293–304, http://dx.doi.org/10.1088/0370-1328/78/2/315.
[8] R.H. Dean, A.B. Dreeben, J.F. Kaminski, A. Triano, Travelling-wave amplifier using thin epitaxial GaAs layer, Electron. Lett. 6 (1970) 775–776, http://dx.doi.org/10.1049/el:19700537.
[9] K. Kumabe, H. Kanbe, GaAs travelling-wave amplifier, Int. J. Electron. 58 (1985) 587–611, http://dx.doi.org/10.1080/00207218508939056.
[10] M. Shur, Physics of Semiconductor Devices, Prentice Hall, 1990.
[11] A.L. Kalapusha, N.Y. Kotsarenko, G.E. Chaika, Possibility of laser-radiation control by space-charge waves in semiconductor-films, Ukr. Fiz. Zh. 33 (1988) 16–18.
[12] V.V. Bryksin, P. Kleinert, M.P. Petrov, Theory of space-charge waves in semiconductors with negative differential conductivity, Phys. Solid State 45 (2003) 2044–2052, http://dx.doi.org/10.1134/1.1626736.
[13] B. Hilling, T. Schemme, K.M. Voit, H.J. Schmidt, M. Imlau, Space-charge wave excitation by superposition of static and moving interference patterns, Phys. Rev. B 80 (2009) 1–5, http://dx.doi.org/10.1103/PhysRevB.80.205118.
[14] P. Kleinert, Space-charge waves in semiconductors excited by static and moving optical interference patterns, J. Appl. Phys. 97 (2005) http://dx.doi.org/10.1063/1.1884250.
[15] B.I. Sturman, Space-charge wave effects in photorefractive materials, in: Photorefractive Mater. Their Appl., Vol. 1, Springer-Verlag, New York, 2006, pp. 119–162, http://dx.doi.org/10.1007/0-387-25192-8_5.
[16] S. Koshevaya, V. Grimalsky, J. Escobedo-Alatorre, M. Tecpoyotl-Torres, Superheterodyne amplification of sub-millimeter electromagnetic waves in an n-GaAs film, Microelectron. J. 34 (2003) 231–235, http://dx.doi.org/10.1023/A.
[17] V.V. Grimalsky, S.V. Koshevaya, Y.G. Rapoport, Superheterodyne amplification of electromagnetic waves of optical and terahertz bands in gallium nitride films, Radioelectron. Commun. Syst. 54 (2011) 401–410, http://dx.doi.org/10.3103/s0735272711080012.
[18] A.A. Barybin, A.I. Mikhailov, Parametric interaction of space-charge waves in thin-film semiconductor structures, Tech. Phys. 45 (2000) 189–193, http://dx.doi.org/10.1134/1.1259595.
[19] A.A. Barybin, A.I. Mikhailov, Parametric interaction of space-charge waves in asymmetric thin-film n-GaAs structures, Tech. Phys. 48 (2003) 761–767, http://dx.doi.org/10.1134/1.1583832.
[20] V. Grimalsky, S. Koshevaya, Nonlinear interaction of terahertz and optical waves in nitride films, Terahertz Sci. Technol. (TST) 6 (2013) 165–176, http://dx.doi.org/10.11906/TST.165-176.2013.09.10.
[21] D.G. Sannikov, D.I. Sementsov, Waveguide interaction between light and an amplified space-charge wave, Phys. Solid State 49 (2007) 488–492, http://dx.doi.org/10.1134/s1063783407030171.
[22] D.G. Sannikov, D.I. Sementsov, Collinear interaction of light with space-charge waves in a semiconductor waveguide, J. Commun. Technol. Electron. 51 (2006) 677–684, http://dx.doi.org/10.1134/s106422690606009x.

[23] D.I. Sementsov, D.G. Sannikov, Transformation of waveguide modes by intensifying space-charge waves, Dokl. Phys. 53 (2008) 40–44, http://dx.doi.org/10.1134/S1028335808090048.
[24] D.G. Sannikov, D.I. Sementsov, Bragg reflection from space charge waves in a semiconductor waveguide, Tech. Phys. Lett. 32 (2006) http://dx.doi.org/10.1134/S1063785006030278.
[25] D.I. Sementsov, D.G. Sannikov, Collinear interaction of optical waveguide modes with an increasing space-charge wave, Opt. Spectrosc. 102 (2007) http://dx.doi.org/10.1134/S0030400X07040194, English Transl. Opt. i Spektrosk.
[26] Y. Zhong, P.B. Dongmo, L. Gong, S. Law, B. Chase, D. Wasserman, J.M.O. Zide, Degenerately doped InGaBiAs:Si as a highly conductive and transparent contact material in the infrared range, Opt. Mater. Express 3 (2013) 1197–1204, http://dx.doi.org/10.1364/OME.3.001197.
[27] J. Hu, J. Meyer, K. Richardson, L. Shah, Feature issue introduction: mid-IR photonic materials, Opt. Mater. Express 3 (2013) 1571–1575, http://dx.doi.org/10.1364/ome.3.001571.
[28] M.E. Levinstein, Y.K. Pozhela, M.S. Shur, Gunn Effect, Sov. Radio, Moscow, 1975, p. 288 (in Russian).
[29] J.E. Caroll, Hot Electron Microwave Generators, Hodder & Stoughton Educational, London, 1970.
[30] N.S. Davydova, Y.Z. Daniushevsky, Diode Generators and Microwave Amplifiers, Radio i Svyaz, Moscow, 1986 (in Russian).
[31] G.E. Chaika, V.N. Malnev, M.I. Panfilov, Diffraction of light radiation on space-charge waves, Opt. Spectrosc. 81 (1996) 437–439.
[32] R.G. Hunsperger, Integrated Optics: Theory and Technology, sixth ed., Springer, New York, 2009.
[33] M.J. Adams, An Introduction to Optical Waveguides, John Wiley & Sons, New York, 1981.
[34] D.G. Sannikov, Waveguide properties of planar structures based on the left-handed media, 2012, http://dx.doi.org/10.4028/www.scientific.net/SSP.190.601.
[35] A. Yariv, Quantum Electronics, third ed., John Wiley & Sons, New York, 1975.
[36] A. Yariv, P. Yeh, Optical Waves in Crystals, John Wiley & Sons, New York, 1984.
[37] W. Streifer, D.R. Scifres, R.D. Burnham, TM-Mode coupling coefficients in guided-wave distributed feedback lasers, IEEE J. Quantum Electron. 12 (1976) 74–78, http://dx.doi.org/10.1109/JQE.1976.1069108.
[38] I. Panyaev, Y. Dadoenkova, I. Zolotovskii, D. Sannikov, Difference frequency generation of narrow-band THz radiation on the basis of a parametric three-wave interaction in a ZnTe crystal, Opt. Commun. 426 (2018) 395–400, http://dx.doi.org/10.1016/j.optcom.2018.05.064.
[39] Y.S. Dadoenkova, I.O. Zolotovskii, I.S. Panyaev, D.G. Sannikov, Difference-frequency generation of THz radiation via parametric three-wave interaction in CdTe and ZnTe crystals, Opt. Spectrosc. 124 (2018) http://dx.doi.org/10.1134/S0030400X18050053, English Transl. Opt. i Spektrosk.
[40] I.O. Zolotovskii, D.A. Korobko, R.N. Minvaliev, D.I. Sementsov, Parametric wave interaction in media exhibiting quadratic and cubic nonlinearities under high-frequency pumping conditions, Opt. Spectrosc. 116 (2014) 110–114, http://dx.doi.org/10.1134/S0030400X14010263.
[41] T. Skauli, P.S. Kuo, K.L. Vodopyanov, T.J. Pinguet, O. Levi, L.A. Eyres, J.S. Harris, M.M. Fejer, B. Gerard, L. Becouarn, E. Lallier, Improved dispersion relations for GaAs and applications to nonlinear optics, J. Appl. Phys. 94 (2003) 6447–6455, http://dx.doi.org/10.1063/1.1621740.
[42] S. Adachi, Optical dispersion relations for GaP, GaAs, GaSb, InP, InAs, InSb, AlxGa1-xAs, and In1-xGaxAsyP1-y, J. Appl. Phys. 66 (1989) 6030–6040, http://dx.doi.org/10.1063/1.343580.
[43] A. Yariv, P. Yeh, Photonics: Optical Electronics in Modern Communications, sixth ed., Oxford University, 2007.
[44] W.D. Kimura, Tunable CO2 laser system with subnanosecond-pulse-train output, Opt. Laser Technol. 88 (2017) 263–274, http://dx.doi.org/10.1016/j.optlastec.2016.09.022.
[45] V.N. Bel'tyugov, A.A. Kuznetsov, V.N. Ochkin, N.N. Sobolev, Y.V. Troitskiĭ, Y.B. Udalov, Waveguide CO2 laser with a selector utilizing a lens and tunable in a frequency band exceeding the resonator intermode spacing, Sov. J. Quantum Electron. 19 (1989) 1347–1352, http://dx.doi.org/10.1070/qe1989v019n10abeh009246.
[46] V.N. Bel'tyugov, A.A. Kuznetsov, V.N. Ochkin, N.N. Sobolev, Y.V. Troitskiĭ, Y.B. Udalov, Use of combined resonators in widening the continuous tuning band of the emission frequency of gas lasers, Sov. J. Quantum Electron. 16 (1986) 610–612, http://dx.doi.org/10.1070/qe1986v016n05abeh006597.
[47] A.M. Ardila, O. Martínez, M. Avella, J. Jiménez, B. Gérard, J. Napierala, E. Gil-Lafon, Temperature dependence of the Raman shift in GaAs conformal layers grown by hydride vapor phase epitaxy, J. Appl. Phys. 91 (2002) 5045–5050, http://dx.doi.org/10.1063/1.1462849.
[48] I. Gravé, M. Segev, A. Yariv, Observation of phase conjugation at 10.6 μm via intersubband third-order nonlinearities in a GaAs/AlGaAs multi-quantum-well structure, Appl. Phys. Lett. 60 (1992) 2717–2719, http://dx.doi.org/10.1063/1.106854.
[49] M. Segev, I. Gravé, A. Yariv, Demonstration of the optical Kerr effect at 10.6 μm via intersubband nonlinearities in a multi-quantum well structure, Appl. Phys. Lett. 61 (1992) 2403–2405, http://dx.doi.org/10.1063/1.108178.
[50] R.W. Boyd, Nonlinear Optics, third ed., Elsevier, New York, 2007.
[51] A.P. Sukhorukov, Nonlinear Wave Interactions in Optics and Radio Physics, Nauka, Moscow, 1988 (in Russian).
[52] W.T. Tsang (Ed.), Semiconductors and Semimetals, Vol. 22. Lightwave Communications Technology. Part E. Integrated Optoelectronics, Academic Press, New York, 1985.
[53] L.A. Eyres, P.J. Tourreau, T.J. Pinguet, C.B. Ebert, J.S. Harris, M.M. Fejer, L. Becouarn, B. Gerard, E. Lallier, All-epitaxial fabrication of thick, orientation-patterned GaAs films for nonlinear optical frequency conversion, Appl. Phys. Lett. 79 (2001) 904–906, http://dx.doi.org/10.1063/1.1389326.
[54] K.L. Vodopyanov, O. Levi, P.S. Kuo, T.J. Pinguet, J.S. Harris, M.M. Fejer, B. Gerard, L. Becouarn, E. Lallier, Optical parametric oscillation in quasi-phase-matched GaAs, Opt. Lett. 29 (2004) 1912, http://dx.doi.org/10.1364/OL.29.001912.
[55] K.L. Vodopyanov, M.M. Fejer, X. Yu, J.S. Harris, Y.-S. Lee, W.C. Hurlbut, V.G. Kozlov, D. Bliss, C. Lynch, Terahertz-wave generation in quasi-phase-matched GaAs, Appl. Phys. Lett. 89 (2006) 141119, http://dx.doi.org/10.1063/1.2357551.
[56] J.J. Pigeon, S.Y. Tochitsky, C. Gong, C. Joshi, Supercontinuum generation from 2 to 20 μm in GaAs pumped by picosecond CO_2 laser pulses, Opt. Lett. 39 (2014) 3246–3249, http://dx.doi.org/10.1364/ol.39.003246.